Solid State Ionics 380 (2022) 115922

Contents lists available at ScienceDirect

Solid State Ionics

journal homepage: www.elsevier.com/locate/ssi

Oxygen diffusion coefficient and characterization of leachant in UO_2 corrosion studied by new methods

L.J. Bonales [a,*], N. Rodríguez-Villagra [b], A. Milena-Pérez [b], M.C. Jimenez Ramos [c], J. García Lopez [c,d], J. Cobos [e,b]

[a] Centro de Astrobiología (CSIC-INTA), Ctra. Ajalvir km. 4, 28850 Madrid, Spain
[b] CIEMAT, Departamento de Energía, Unidad de Residuos de Alta Actividad, Av. Complutense, 40, 28040 Madrid, Spain
[c] CNA (U. Sevilla, J. Andalucia, CSIC), Av. Thomas A. Edison 7, 41092 Sevilla, Spain
[d] Dept. Física Atómica, Molecular y Nuclear, Universidad de Sevilla, Av. Reina Mercedes s/n, 41012 Sevilla, Spain
[e] Estación Biológica de Doñana (EBD-CSIC), Avda. Américo Vespucio 26, 41092 Sevilla, Spain

ARTICLE INFO

Keywords:
UO_2
Corrosion
Oxygen diffusion coefficient
Oxidized layer thickness

ABSTRACT

UO_2 corrosion is a key issue in the study of the safe storage of spent nuclear fuel (SNF). In this work, corrosion experiments were performed on UO_2 samples exposed to ^{18}O labelled water during 290 days at room conditions, thereafter a complete analysis of the solid and leachant (labelled water) allow us obtaining new data and exploring new methods.

Thus, a new application of the Nuclear Reaction Analysis (NRA), as a simple and low-cost approach, has been developed to estimate the oxidized layer thickness and the diffusion coefficient of oxygen through the oxidized layer. These results were verified by comparison with the ones obtained by traditional Secondary Ion Mass Spectrometry (SIMS).

The diffusion coefficient obtained is two orders of magnitude larger than the scarce published ones at room temperature, highlighting the great effect of the composition of the oxidized layer due to the UO_2 corrosion on this parameter. In addition, the water used in the corrosion experiments (leachant) has been analyzed by Raman spectroscopy, being the main purpose for the *in situ* analysis.

The data obtained in this study bring out the great ability (higher than expected) of the oxygen to break through the oxidized layer which could endanger the SNF pellet integrity.

Besides, this work shows new methods for analyzing corrosion experiments which can be used to obtain new data for completing the database.

1. Introduction

The behavior of the spent nuclear fuel (SNF) in geological repository conditions is a matter of concern for the international scientific community, since this storage is considered the best option for the final management of the nuclear waste [1]. The challenge is to ensure safe repository conditions to avoid the radionuclides reaching the biosphere over a long time scale in the order of millions of years (time needed for the radioactivity to decrease to the natural uranium level) [2]. Since the radionuclides are trapped into the spent fuel matrix structure, constituted by uranium dioxide, the stability of the UO_2 plays a crucial role, and has to be assessed under possible conditions and events in a long-term geological repository [3, 4].

It is widely recognized that SNF will be in contact with groundwater when the engineered barriers that protect the waste will be breached (either due to aging or if an accident occurs) and, because of that, the reactions of water with uranium dioxide have been undertaken in several previous works [5–13].

At the same time, water radiolysis alters the chemistry of water and induces oxidative dissolution of SNF by radiolytic decomposition of water, in a process that creates oxidizing species, which in turn increase the oxidative dissolution of UO_2 [14], transforming reducing environments into oxidizing ones [15, 16].

Senanayake et al. [17] studied by high resolution XPS from the X-ray synchrotron light and temperature programed desorption (TDP) the interaction of water vapor on the surface of the uranium dioxide at 300

* Corresponding author.
E-mail address: ljbonales@cab.inta-csic.es (L.J. Bonales).

https://doi.org/10.1016/j.ssi.2022.115922
Received 5 August 2021; Received in revised form 1 April 2022; Accepted 4 April 2022
Available online 9 April 2022

K. As for hypostoichiometric uranium oxide, UO_{2-x}, adsorption and dissociation of water take place forming H_2 and O_2, whereas for stoichiometric UO_2 this adsorption is reversible and no H_2 was detected.

In the same line, these authors [17] reported that oxidation from UO_2 to U_3O_8 occurred with water vapor at 300 K by analyzing the surface with Raman spectroscopy. This reaction is generally described as a two-step reaction [18], $UO_2 \rightarrow U_4O_9$ / $U_3O_7 \rightarrow U_3O_8$, with an increase of around 36% in volume, which might affect the integrity of the fuel pellets and therefore the potential release of radionuclides [19].

Matzke and Turos [20] studied the kinetics of formation and growth of uranium oxides layers of U_3O_7 and U_2O_5, during leaching experiments in distilled water, from room temperature to 200 °C, and different times ranging from 1 h to 1000 h. At $T < 130$ °C they did not find any oxidation layer, but for higher temperatures (200 °C) and times between 600 and 1000 h, they found the precipitation of schoepite ($UO_3{\cdot}nH_2O$). Experimental data at $T > 150$ °C were modelled with the Monte Carlo channeling simulations [21].

Therefore, the interaction of water with UO_2 can be described by an oxidative dissolution mechanism *via* two reactions: 1) oxidation of U^{4+} to U^{6+} at UO_2 surface forming layers of different oxides ($UO_2 \rightarrow U_3O_8$) in presence of oxidants such as oxygen followed by the subsequent formation of the uranyl aqueous specie (UO_2^{2+}) and 2) precipitation of secondary phases, containing uranyl groups, UO_2^{2+}, in their structures [22–24].

The first reaction is T-depending following an Arrhenius behavior, and it is controlled by the diffusion of O_2 through the oxidized layer [20]. The diffusion coefficient of O_2 and the penetration of water at room temperature are normally extrapolated from experiments performed at high temperatures. The only empirical data at low temperature (~ 25 °C and 60 °C) have been reported in the experiments conducted by Marchetti et al. [25–28].

The second reaction is usually studied analyzing the alteration products of uraninite [29–32] and being the studies of schoepite in leaching experiments at controlled conditions scarce [33].

In this work, we study the two aforementioned reactions by performing static leaching essays on UO_2 discs using ^{18}O labelled water at room temperature (~ 25 °C), in order to reproduce the expected conditions of the geological repository. The results of this study are organized as follows: First, the oxidized surface of the UO_2 discs and the secondary phases precipitated at the UO_2 surface are characterized by using traditional techniques (scanning electron microscopy, Raman spectroscopy and X-ray diffraction). Secondly, the depth profile of the oxidized layer and the Oxygen diffusion coefficient are both estimated by using a new application of the Nuclear Reaction Analysis (NRA). The results were verified by comparing them with those obtained by Secondary ion mass spectrometry (SIMS), following the method published by Marchetti et al. [28]. Thirdly, a new protocol to evaluate the leaching based on Raman spectroscopy is introduced.

2. Materials and methods

2.1. Static leaching experiment

An unirradiated UO_2 pellet provided by ENUSA with a diameter of 10.4 mm was cut into discs with parallel faces of ~1 mm-thickness. In order to ensure initial stoichiometry, UO_2 samples were annealed at 800 °C during 24 h under reducing conditions (N_2:H_2 95.3:4.7%*v*/v). The pre-leaching characterization was done by using X-ray diffraction (XRD), Raman spectroscopy and scanning electron microscopy (SEM).

Static corrosion tests were carried out by contacting two UO_2 discs (0.7–0.8 g) with 16–17 mL of deionized water in small vials under oxygen-free atmosphere (Ar). The experiments were conducted in a glass vessel with 91% ^{18}O labelled water (calculated by weight), at room temperature (22–27 °C), for 290 days.

After this time supernatant was removed from disc 1 and solid sample was quickly air-flow dried. Water from disc 2 was left to evaporate slowly at room temperature. Both solids were kept at inert conditions until further analysis.

2.2. Raman spectrometer

A Horiba LabRam HR evolution spectrometer (Jobin Yvon Technology) was used for Raman spectroscopy analysis. A red laser of HeNe with a wavelength of 632.81 nm and an operation power of 20 mW was used as the excitation source. The laser was focused onto the sample using a 100× objective at the confocal microscope BX4 with 800 mm confocal; the scattered light was collected with the same objective and then dispersed with a Jobin-Yvon spectrometer (600 grooves / mm), and detected with a Peltier cooled CCD detector (256 × 1024 pix.). The spatial resolution was less than 1 μm, and the spectral resolution was about 1 cm^{-1}/ pixel.

2.3. X-ray diffraction

For the XRD patterns, a Philips PANalytical X'Pert MPD diffractometer (40 kV and 45 mA) mounted in a Bragg-Brentano configuration with Cu $K_{\alpha 1}$ radiation (λ = 1.54056 Å) was used. The diffraction patterns were recorded within the 20° to 120° range (2θ), with a counting step of 0.02°.The total measuring time was 18 h.

2.4. Scanning electron and optical microscopy

In regard to SEM analysis, a HITACHI S2500 device operating at 25 kV was used to characterize surface morphology. The leached specimens were placed onto an aluminum sample holder and secured using adhesive tape carbon to promote conductivity between the pads and the holder. Since UO_2 pellets are semiconductor the metallic coating was not necessary.

Optical images were acquired with an Olympus BX41 microscope provided with several long-distance Olympus objectives of different magnification (5×, 10×, 50×) and a cold source for illumination.

2.5. Nuclear reaction analysis (NRA)

The atomic concentration and depth profile of ^{18}O into the UO_2 pellets was determined by NRA using the 3 MV Tandem accelerator of the National Accelerator Center. The $^{18}O(p, \alpha)^{15}N$ nuclear reaction was employed, with a proton beam energy of 771 keV. The proton beam current at the target was 40 nA over a spot of about 3 mm in diameter to induce the nuclear reaction. The energy spectra of the released α particles were recorded using a Canberra PIPS detector set at the scattering angle θ = 150°. A $Si^{18}O_2$/Si target with 374 × 10^{15} atoms $^{18}O/cm^2$ was used as a reference sample. The NRA spectra were analyzed with the SIMNRA code. To convert the units of atoms/cm^2 measured by NRA into units of depth, the density of bulk UO_2 was used (ρ = 10.38 g/cm^3 = 6.95 × 10^{22} at/cm^3). That means that 1000 × 10^{15} at/cm^2 of UO_2 corresponds to a depth of approximately 144 nm.

2.6. Secondary ion mass spectrometry (SIMS)

SIMS (HIDEN SIMS Workstation) depth profile was performed using a quadrupole instrument (MAXIM 1000 + DETECTOR (ion counting)), with an oxygen O_2^+, Ar primary beam at near normal incidence. In this work a primary ion energy of 0.5–5 keV, and current of 0.1–600 nA were used. An area of 36 mm^2 with a beam spot size of 20–50 μm was scanned. The sputter time was converted to depth by profilometry. Here, a linear dependence of the count yield with concentration was assumed.

3. Results and discussion

3.1. Surface characterization

Pre- and post-corrosion surface characterization of both leached UO_2 discs was performed by means of SEM and optical microscopy in order to assess the surface morphology (Fig. 1). XRD and Raman spectroscopy analyses of initial and post treated sample were also performed (Figs. 2 and 3 respectively).

Fig. 1.a revealed a homogeneous UO_2 surface with no evidence of micro cracks or defects on the pellet surface, and a homogenous grain size of around 8–10 μm. This image, obtained in a pre-leached disc, stands in contrast to the SEM images of the UO_2 disc 1 and 2 (Fig. 1.b and 1.c, respectively) after leaching reaction where the grains are significantly more smoothed, presumably due to the oxidative dissolution. Post-leached SEM image of UO_2 disc 2 exposed to ^{18}O-labelled water and air-evaporated without removing the leachant is shown in Fig. 1.c. In this figure, precipitation of a yellow secondary phase on the UO_2 surface is observed to the naked eye at the end of the drying process. This precipitated phase is composed by rectangular crystals of size edges ranging from 2 to 5 μm.

X-ray diffraction patterns of the pre- and post- leached surface of UO_2 and of the secondary phase precipitated are shown in Fig. 2.a, b and c, respectively.

Fig. 2.a shows the typical XRD pattern in the 25–40° 2θ range of the cubic structure of stoichiometric UO_2, in agreement with the published data by Fritsche et al. [34], and represented by open symbols in the figure (ICCD 00–41–1422). Assuming the Fm-3 m space group for UO_2, the empirical lattice parameter was 0.54706 nm, in agreement with the value reported in literature of 0.5470 nm [35, 36].

The diffraction pattern in the 2θ angle range of 25–40° in Fig. 2.b corresponds to a mixture of uranium oxides with different oxidation degrees. Accordingly, it can be understood as a mixture of hyper-stoichiometric UO_{2+x} with $0 < x < 0.25$ (ICDD 01–071-0258) and U_3O_8 (ICDD 00–047-1493), see caption in figure. Cell parameter of UO_{2+x} was of 0.5450 nm, thus the oxidation degree (x) is $x = 0.22$ by using the Vegard's law.

U_3O_8 is described as an orthorhombic structure, with space group C2mm. The analysis of the pattern shown in Fig. 2.b provides values of a = 1.1926 nm, b = 0.6721 nm c = 0.8290 nm in good agreement with the values estimated by other authors [37].

The pattern in Fig. 2.c shows a mixture of uranium oxides with different oxidation degree and, as described above, peaks fit with the metaschoepite pattern, (see symbols corresponding to the ICCD 01–089-7333), published in [38]. Metaschoepite, $[(UO_2)_8O_2(OH)_{12}]\cdot 10H_2O$, has an orthorhombic structure with space group Pbna. As it is well-known, this secondary phase is obtained by the slow dehydration of schoepite $[(UO_2)_8O_2(OH)_{12}]\cdot 12H_2O$in air at ambient temperature. Due to the difficulties in distinguishing these phases on the basis of X-ray power diffraction data alone [38], here we use the name schoepite for the phase close to $UO_3\cdot 2H_2O$.

Fig. 3 shows some results of the Raman characterization. The spectrum of stoichiometric UO_2 is shown in Fig. 3.a, which corresponds to the pre-leached sample. After leaching, the spectra obtained are associated with the typical spectrum of UO_{2+x} ($0 < x < 0.25$) and U_3O_8, (Fig. 3.b). Fig. 3.c shows a spectrum with the most intense bands around 800 cm^{-1}, feature and fingerprint for most of the U^{6+} minerals [39] and assigned to the symmetric stretching vibration of UO_2^{2+} group, $\nu_1(UO_2)^{2+}$.

The spectrum corresponding to the pre-leached sample has two bands at 445 and 1150 cm^{-1} (see Fig. 3.a) [40–42]. The first one is assigned to the U—O fundamental stretching vibration and the second one corresponds to the 2LO phonon band. The three bands in the range of 300–500 cm^{-1} and the band at 812 cm^{-1} show that U_3O_8 is reached after leaching (see Fig. 3.b) [43, 44]. Finally, Fig. 3.c shows one of the spectra obtained from the crystal structures precipitated at the surface after leaching experiments. The spectrum corresponds to the typical one of schoepite, *i.e.* two strong Raman bands at 842 and 857 cm^{-1} which are both attributed to the symmetric stretch, ν_1, owing to the fact that the uranyl ion is postulated to be present in two nonequivalent sites [45–47] (see Table 1).

In addition to these strong signals, schoepite spectrum also presents weak signals between 300 and 500 cm^{-1} which can be attributed to the ν(U—O) at the equator of the uranyl ion (UO_2^{2+}).

3.2. Oxidized layer thickness and profile

In this section, an estimation of the depth of the oxidized layer, λ, in altered UO_2 disc 1 was assessed by new application of the Nuclear Reaction Analysis (NRA). The depth profile results were checked by a comparison with the ones obtained by Secondary Ion Mass Spectrometry (SIMS), following the method published by Marchetti et al. [28]. These two techniques were used to deduce the oxygen diffusion coefficient in the UO_2 altered surface.

3.2.1. Nuclear reaction analysis (NRA)

In order to know the in-depth oxygen distribution along the profundity of the sample, the $^{18}O(p, \alpha)^{15}N$ nuclear reaction was applied. In Fig. 4, the energy spectra from NRA is presented, including both the experimental (black dots) and simulated (red line) data. The signal produced by the alpha particles, coming from the nuclear reactions with the atoms present at the surface of the sample, is clearly visible in the region of energy 800–1600 keV. Below this energy, the alpha signal overlaps with an important background due to the backscattered protons with the U atoms (not shown). This means that the maximum depth that we can explore is ~850 nm. For the simulation, a UO_2 target was assumed, the only free parameter was the depth profile of the ^{18}O relative isotopic abundance, [^{18}O] (for natural oxygen, [^{18}O] = 0.2%). As can be observed in Fig. 4, the sample presents an enriched layer at the surface (1600–1400 keV), with a maximum value of [^{18}O] = 1.75 ±

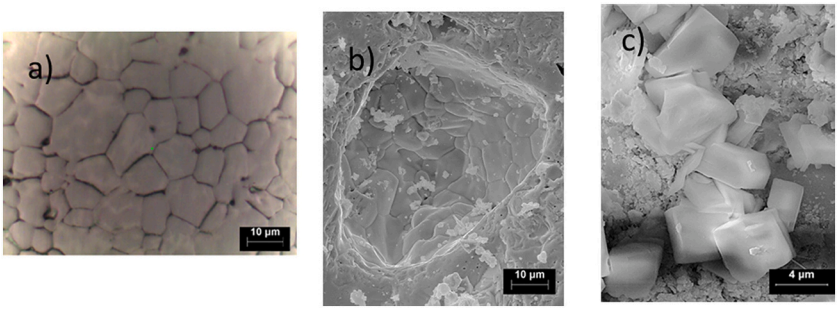

Fig. 1. Optical and SEM images of the UO_2 discs surface before and after corrosion in presence of ^{18}O-labelled water. The original UO_2 surface before the leaching experiment is shown in image (a) by optical microscopy. The sharp-edged UO_2 grains and grain boundaries are observable. The SEM images of disc 1 and disc 2 UO_2 surface after leaching experiments are respectively given in (b) and (c).

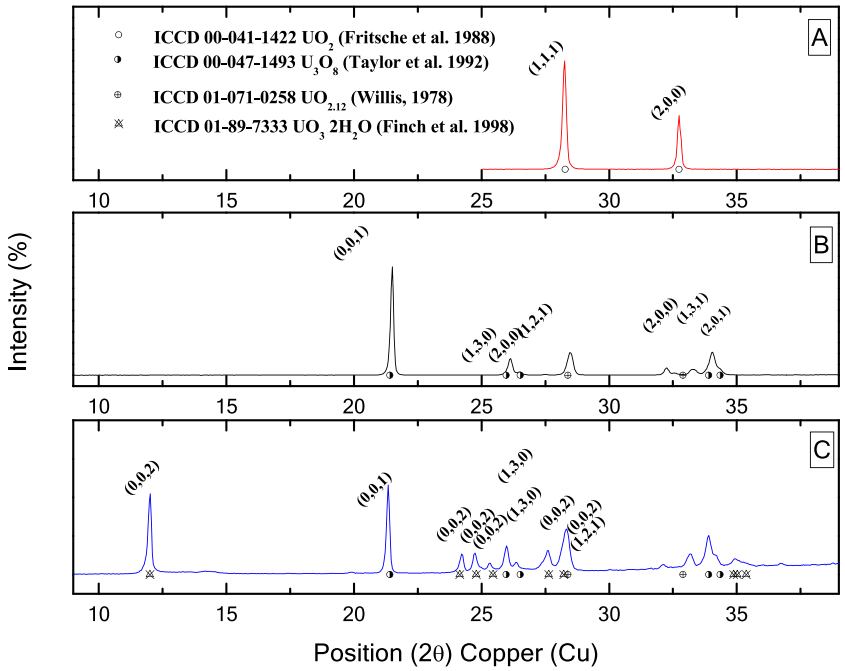

Fig. 2. X-ray powder diffraction pattern of the UO_2 disk surface (a) before leaching showing the characteristic peaks of uraninite; (b)after leaching of the disc 1, corresponding to a partially oxidized sample; and (c) of the disc 2, revealing the presence of a mixture of uranium oxides and metaschoepite.

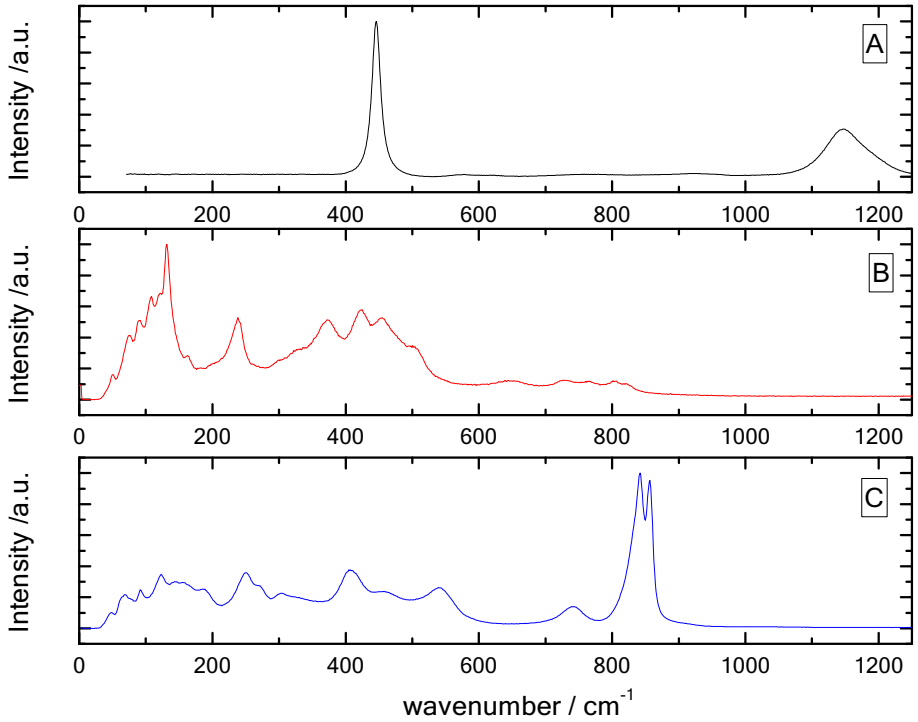

Fig. 3. Raman spectra of UO_2 leaching experiments in presence of ^{18}O-labelled water: a) pre-leached UO_2 surface, (b) after leaching of the disc 1, once the leachate is removed, and (c) of the crystalline structures precipitated at the surface of the disc 2.

0.05% that decays with depth, followed by a virtually constant background with $[^{18}O] = 0.6 \pm 0.1\%$. The better precision obtained for the surface concentration compared to the bulk concentration is mainly due to the higher counting statistics in this region. The drop of the signal between 1400 and 800 keV reflects the energy dependence of the $^{18}O(p, \alpha)^{15}N$ cross section. Neglecting the impact of surface roughness and assuming direct lattice diffusion to be the main phenomenon governing the experimental profile in this region, the classic solution of Fick's law [53] can be used to fit the results of the NRA analysis according to Eq. 1.

$$C(x) = C_B + 1.2\ erfc\left(\frac{x}{\lambda_{NRA}}\right), \quad (1)$$

where C(x) is the ^{18}O relative isotopic abundance ($[^{18}O]$) measured by NRA, C_B = 0.6% is the $[^{18}O]$ bulk background and *erfc* is the

Table 1
Raman shifts of the $\nu_1(UO_2)^{2+}$ symmetric stretching vibrations reported in the literature.

Raman shift (cm^{-1})	Reference
875/868	Lu et al. 2018 [48]
855/838	Stefaniak et al. 2008 [49]
838/855	Frost et al. 2006 [50]
855/843	Mellini et al. 2005 [51]
843/855	Amme et al. 2002 [47]
840/860	Biwer et al. 1990 [46]
846/870	Hoekstra and Siegel 1973 [52]
844	Maya and Begun 1981 [45]
841.9/856.9	This work

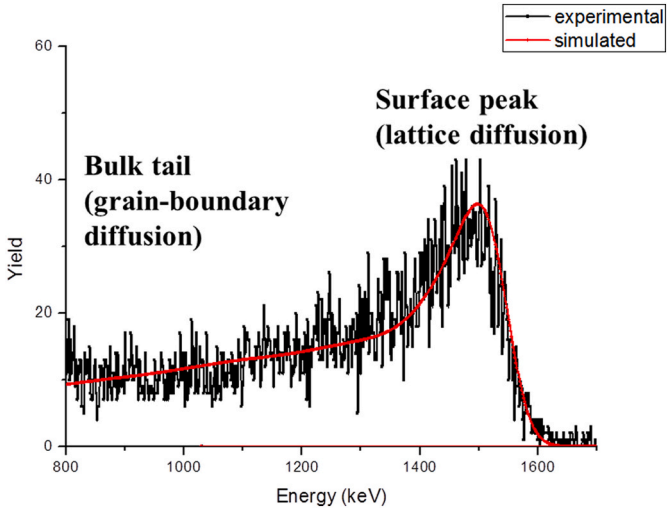

Fig. 4. NRA spectrum of oxidized UO_2 disc showing a surface peak and a long-range diffusion profile. Red curve corresponds to the simulation using the SIMNRA code. (For interpretation of the references to colour in this figure legend, the reader is referred to the web version of this article.)

complementary error function

$$erfc(z) = \frac{2}{\sqrt{\pi}} \int_z^{\infty} e^{-t^2} dt$$

Note that erfc (0) = 1 so the factor 1.2 is introduced to obtain the correct [^{18}O] value (≈1.8%) at the surface. Using Eq. 1, the calculated depth of the oxidized layer is $\lambda_{NRA} = 150 \pm 10$ nm.

The NRA spectra were fitted using the SIMNRA program, which allows to evaluate the goodness of fit by means of an χ^2 analysis, where χ^2 is the quadratic deviation between experimental and simulated data.

$$\chi^2 = \sum_i \frac{\left(N_{exp}(i) - N_{sim}(i)\right)^2}{\sigma_i^2} \quad (2)$$

The reduced χ^2_r is defined as χ^2/N were N is the number of channels. The χ^2_r value for the NRA spectrum shown in Fig. 4 is $\chi^2_r = 1.2$.

3.2.2. Secondary ion mass spectrometry (SIMS)

The depth of the oxidized layer can also be estimated by SIMS analysis as evidenced by Marchetti et al. [28].

Fig. 5.a shows the typical raw depth profiles, *i.e.* the intensity of the signal of each mass in counts per second (cps), as a function of the sputtering time in ms. Time scale of the raw depth profiles was converted to depth scale by means of a calibration of the sputtering rate of the sample by profilometry.

The ^{18}O relative isotopic abundance, *c(x),* was calculated following Eq. 3.

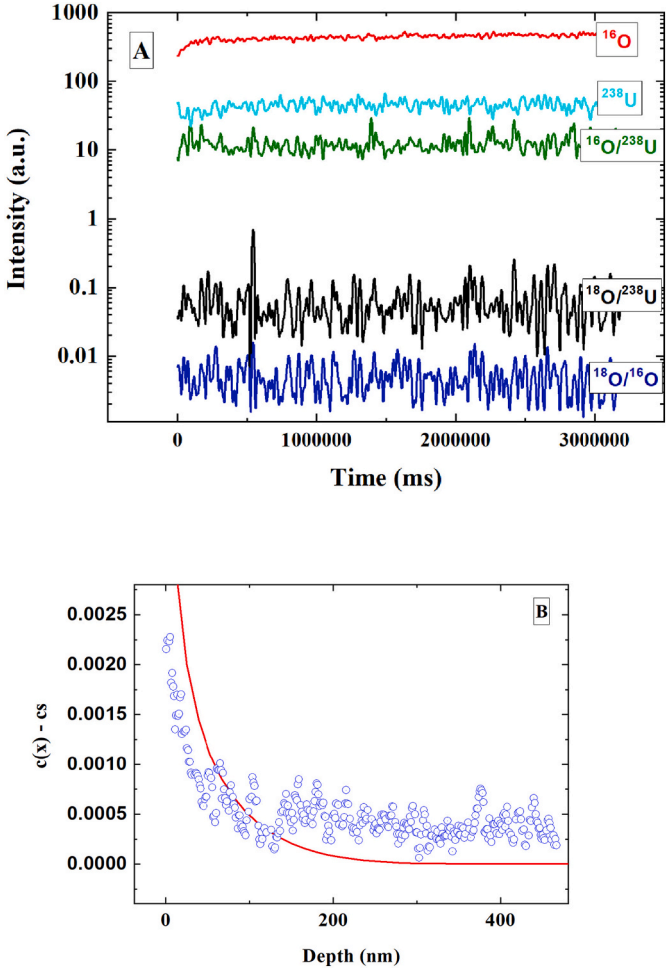

Fig. 5. (a) SIMS raw data of depth profiling for different mass, ^{16}O, ^{238}U, ^{16}O / ^{238}U, ^{18}O/^{238}U, ^{18}O/^{16}O. (b) SIMS short –range diffusion profiles (open points) in terms of the ^{18}O relative isotopic abundance including c(x) fit (line) to Eq. 1. ($R^2 = 0.65$).

$$c(x) = I\left(^{18}O\right) / \left[I\left(^{18}O\right) + I\left(^{16}O\right)\right], \quad (3)$$

where *I* is the measured secondary ion current, *vs.* the sputtering depth, *x* (Fig. 5.b).

Neglecting the impact of surface roughness and assuming direct lattice diffusion to be the main phenomenon governing the experimental profile in this region, the classic solution of Fick's law can also be used in the SIMS analysis to fit the average curve shown in Fig. 5.b (in red).

As can be seen from this same Figure, this model fits well to the profile and from this fit, a diffusion length $\lambda_{SIMS} = 169 \pm 15$ nm is obtained for oxygen after a leaching time of 290 days.

3.3. Diffusion coefficient of oxygen through the oxidized layer

The results observed in the NRA experiments suggest that the oxygen diffusion takes place through two different mechanisms: i) a direct lattice diffusion from the surface giving place to the surface peak, and ii) a faster diffusion known as a grain-boundary diffusion (see Fig. 4). The first one comes from the ^{18}O atoms incorporated and diffused into the grains by the chemical reaction between water molecules and the UO_2 lattice. The second one is the diffusion along grain boundaries, which is characterized by a faster diffusion coefficient D_B, than the one corresponding to the direct lattice diffusion, D_L [26].

The formula used to fit the surface peak corresponds to the classical solution of Fick's law [53], where the parameter λ_{NRA} is the lattice

diffusion length, which can be directly related to the lattice diffusion coefficient, D_L, by.

$$\lambda_{NRA} = 2\ (D_L\ t)^{1/2}, \quad (4)$$

According to the NRA results (λ_{NRA} = 150 nm), the chemical diffusion coefficient D_L for *t* (leaching time = 290 days) is $D_L = 2.2 \cdot 10^{-0.22}$ m^2 /s.

A similar value of the lattice diffusion coefficient is found by using the λ_{SIMS} = 170, which leads a value of $D_L = 2.9\ 10^{-22}$ m^2 / s.

These values of the diffusion coefficient in the lattice are two orders of magnitude higher than the only ones found in literature, corresponding to Marchetti et al. ($D_L = 1.4\ 10^{-24}$ m^2 / s, [26] and $2.5\ 10^{-24}$ m^2 / s [28], although it is compatible with the upper limit of Lay's value (between 10^{-29} and $\cdot 10^{-0.22}$ m^2 /s) [54] based on the Arrhenius fit of data obtained in the temperature range 900–1400 K. Differences found from Marchetti et al. data might be due to the oxidation degree of UO_2 sample. Under the experimental conditions used in both works, the UO_2 samples undergo oxidation. Therefore, the oxygen diffusion coefficients obtained should be referred not to stoichiometric UO_2 ($UO_{2.00}$) but to oxidized UO_2 (UO_{2+x}, U_3O_7, U_4O_9 and/or U_3O_8).

In Fig. 6 the D_L obtained in this work and the ones from refs 25–27, and are plotted along the Arrhenius-type expression of the diffusion coefficients for U_4O_9, U_3O_7 [55] and uraninite [56].

As seen in Fig. 6, D_L values determined in this work can be considered compatible with a mixture of U_3O_7, U_4O_9 and/or uraninite, whereas data from refs 25–27, and can be considered compatible with U_3O_7. In this sense, the diffusion coefficients determined in the different experiments, might actually refer to differently oxidized UO_2 samples due to the fact that the experimental time used in the present work (290 days) is more than three times larger than the one used by the cited bibliography (90 days).

These results are in concordance with the surface characterization shown in section 3.1 (see Figs. 2 and 3), since uraninite mineral, known as the natural analogue of the SNF, is characterized by a mixture of uranium oxides (from UO_2 to U_3O_8), uranyl oxyhydroxides (like schoepite), uranyl silicates and specific alteration products dependent on local conditions [57].

It should be note that the appearance of U_3O_8 leads to an increase in volume of 36%, causing voids and cracks formation where the oxygen existing in water penetrates more easily. More experimental effort must be made in order to evaluate the diffusion coefficient of oxygen through layers of different oxides.

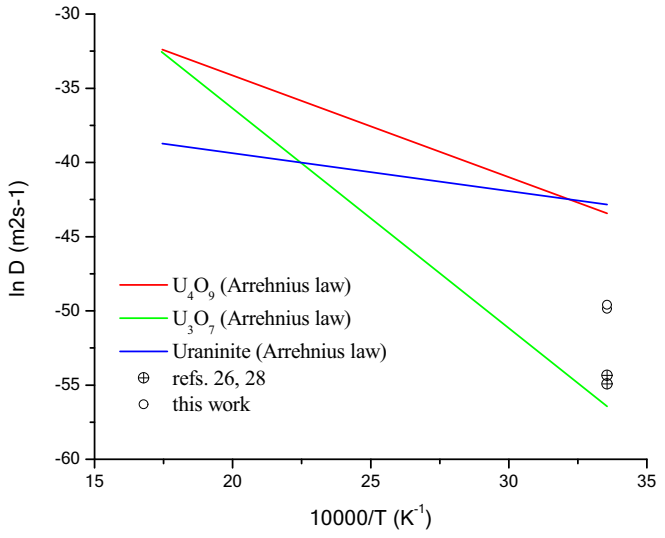

Fig. 6. Comparison of experimental data obtained in this work and from refs 25–27, and with extrapolation given by Poulesquen et al. [55] and Fayek and Kyser [56].

3.4. Leaching analysis by Raman spectroscopy

After the contact of the UO_2 disc (identified as disc 1) with 91% ^{18}O labelled water (calculated by weight) at room temperature during the leaching time (290 days), an aliquot of water was analyzed by Raman spectroscopy, in order to estimate the decrease of ^{18}O due to its transference to UO_2 (oxidation) and forming non-stoichiometric oxides characterized with XRD and Raman.

It is well known that vibrational spectroscopy is a powerful tool to study the effect of the isotopic substitution. This is mainly due to the fact that the normal modes of an isotopically substituted molecule are different to the normal modes of an unsubstituted molecule, leading to different corresponding vibrational frequencies for the substituted atoms.

When an atom is replaced by a heavier isotope, the reduced mass μ increases and leads to a downshift (smaller wavenumber) in the Raman spectrum of the molecule. In order to perform a reliable quantitative analysis of the frequencies shifts, the second derivative of the measured Raman spectra has been computed. Typical obtained Raman spectra of water are presented in Fig. 7.a; together with the second derivative spectra (Fig. 7.b) of the ^{18}O labelled water before and after leaching experiments on UO_2 disc 1 [58]. Fig. 7.b shows the downshifts of the different bands of the water molecule; these shifts due to the isotopic substitution are not visible in the Raman spectra. As seen in Fig. 7.b, the largest displacement experienced by the different bands is observed in the range of 0–400 cm^{-1}, therefore the low wavenumber range is analyzed in order to calculate the decrease of ^{18}O in the leaching reaction.

As can be seen in Fig. 8, a calibration curve has been performed by analyzing the Raman spectrum of water solutions with known concentration ratios of ^{18}O / ^{16}O.

From the linear fit of the plot of the Raman shift low wavenumber range *vs* the isotopic ratio ^{18}O / ^{16}O shown in Fig. 7, the adjust given by Eq. 5 is obtained.

$$\nu_{\text{low frequency}} = 184.4\ (0.6)\ cm^{-1} - 0.11\ (0.01)\ (^{18}O)\% \quad (5)$$

This implies that, by using Eq. 5 on leaching experiment, the obtained value of ^{18}O / ^{16}O is around 60% for 290 days of contact time with 91% ^{18}O labelled water.

This study has thus highlighted that Raman spectroscopy is a powerful tool to study the decrease in the ^{18}O / ^{16}O ratio of UO_2 leaching experiments with ^{18}O labelled water, which is due to the surface oxidation of the UO_2. In this sense, this technique could be used for kinetic studies of dissolution experiments, which becomes particularly important for clarifying different aspects of the matrix corrosion process of UO_2 and provide the basis for further studies.

4. Conclusions

In this work, a study of the UO_2 corrosion with water has been carried out by performing static leaching experiments with ^{18}O labelled water at room conditions during 290 days.

A traditional characterization of the UO_2 surface by using SEM, X-ray diffraction and confocal Raman techniques has shown that the surface of stoichiometric UO_2 oxidizes at the experimental conditions, resulting in a mixture of uranium oxides and the secondary uranyl phase precipitated at on the surface exposed to water, which is identified as Schoepite.

New application of the Nuclear Reaction Analysis has been used to estimate the oxidized layer thickness, λ, and the oxygen diffusion coefficient through the oxidized layer, D_L. This analysis gives a λ_{NRA} = 150 nm which is in agreement with the one obtained by Secondary ion mass spectrometry (SIMS), λ_{SIMS} = 170 nm, by following the method

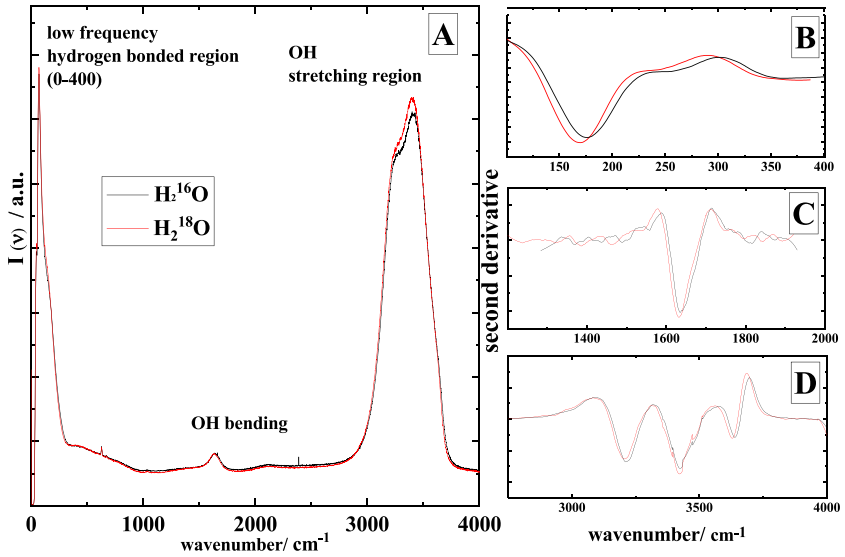

Fig. 7. a) Typical Raman spectrums of water, b-d) the second derivative of the Raman spectra in different regions. Red curves correspond to ^{18}O substituted water after leaching experiments, while the black ones correspond to the unsubstituted water. (For interpretation of the references to colour in this figure legend, the reader is referred to the web version of this article.)

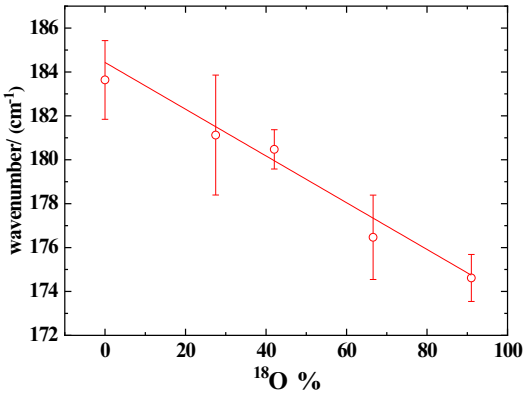

Fig. 8. Calibration curve obtained from the water spectra at different ^{18}O / ^{16}O concentrations.

published by Marchetti [23]. This agreement between λ_{SIMS} and λ_{NRA} values validates this new NRA application. The diffusion coefficient of oxygen D_L has been then estimated, by SIMS and NRA, and it is found to be $D_L(NRA) = 2.2{\cdot}10^{-22}\ m^2$ / s and D_L (SIMS) $= 2.88{\cdot}10^{-22}\ m^2$ / s. These values are higher than those previously published. The discrepancy has been related to the difference in the oxidation degree of the UO_2 surface pellet.

These findings suggest that the oxidized layer of UO_2 has a profound effect of accelerating oxygen through UO_2, which means in a faster loss of the structural integrity than expected, and therefore an earlier release of radionuclides trapped at the UO_2 matrix in the SNF.

Finally, Raman spectroscopy is established as an appropriate additional method for tracking the ^{18}O concentration in labelled water used in leaching experiments. In this sense, a new protocol based on the Raman spectra of the isotopic ratio ^{18}O / ^{16}O evolution is presented, being the key purpose for the *in situ* analysis in this leaching essay.

Authorship contributions

J. Cobos: conception and design of study, acquisition of data and analysis and interpretation of data, revising the manuscript critically for important intellectual content and approval of the version of the manuscript to be published.

J. García Lopez: Acquisition of data and analysis and interpretation of data, revising the manuscript critically for important intellectual content and approval of the version of the manuscript to be published.

M.C. Jimenez Ramos: Acquisition of data and analysis and interpretation of data, revising the manuscript critically for important intellectual content and approval of the version of the manuscript to be published.

A. Milena-Pérez: Revising the manuscript critically for important intellectual content and approval of the version of the manuscript to be published.

N. Rodríguez-Villagra: Revising the manuscript critically for important intellectual content and approval of the version of the manuscript to be published.

L. J. Bonales: Conception and design of study, acquisition of data and analysis and interpretation of data, Drafting the manuscript and approval of the version of the manuscript to be published.

Declaration of Competing Interest

The authors declare that they have no known competing financial interests or personal relationships that could have appeared to influence the work reported in this paper.

Acknowledgments

This investigation was financially supported by ENRESA in the frame of the project: N° 079000189 entitled “Aplicación de técnicas de caracterización en el estudio de la estabilidad del combustible nuclear irradiado en condiciones de almacenamiento” (ACESCO) and by AEI project MDM-546 2017- 0737 Unidad de Excelencia “María de Maeztu”.

References

[1] "Community Policy and Research & Training Activities", EURADWASTE 08, European Commission, Luxembourg, 2008.
[2] SKB 91, Final Disposal of spent nuclear fuel. Importance of the bedrock for safety, SKB Report 92–20, May 1992.
[3] R.C. Ewing, Long-term storage of spent nuclear fuel, Nat. Mater. 14 (2015) 252–256.
[4] D.W. Shoesmith, Fuel corrosion processes under waste disposal conditions, J. Nucl. Mater. 282 (2000) 1–31.

[5] J. Janeczek, R.C. Ewing, L.E. Thomas, Oxidation of uraninite: does tetragonal U_3O_7 occur in nature? J. Nucl. Mater. 207 (1993) 177–191.
[6] R.J. Finch, R.C. Ewing, The corrosion of uraninite under oxidizing conditions, J. Nucl. Mater. 190 (1992) 133–156.
[7] I. Casas, E. Cera, J. Bruno, Kinetic studies of natural uranium minerals for the long-term evolution of spent nuclear fuel under oxidizing conditions, Mater. Res. Soc. Symp. Proc. 294 (1992) 521–525.
[8] S. Sunder, D.W. Shoesmith, M.G. Bailey, F.W. Stanchell, N.S. McIntyre, Anodic oxidation of UO_2: part I. electrochemical and X-ray photoelectron spectroscopic studies in neutral solutions, J. Electroanal. Chem. Interfacial Electrochem. 130 (1981) 163–179.
[9] H. Matzke, Analysis of the structure of layers on UO_2 leached in H_2O, J. Nucl. Mater. 238 (1996) 58–63.
[10] M.E. Torrero, E. Baraj, J. de Pablo, J. Giménez, I. Casas, Kinetics of corrosion and dissolution of uranium dioxide as a function of pH, Int. J. Chem. Kinet. 29 (1997) 261–267.
[11] F.N. Skomurski, J.W. Wang, R.C. Ewing, U. Becker, Charge distribution and oxygen diffusion in hyperstoichiometric uranium dioxide UO_{2+x} ($x<0.25$), J. Nucl. Mater. 434 (2013) 422–433.
[12] F. Gupta, A. Pasturel, G. Brillant, Diffusion of oxygen in uranium dioxide: a first-principles investigation, Phys. Rev. B 81 (2010), 014110.
[13] S.D. Senanayake, G.I.N. Waterhouse, A.S.Y. Chan, T.E. Madey, D.R. Mullins, H. Idriss, The reactions of water vapour on the surfaces of stoichiometric and reduced uranium dioxide: a high resolution XPS study, Catal. Today 120 (2007) 151–157.
[14] M. Jonsson, F. Nielsen, O. Roth, E. Ekeroth, S. Nilsson, M.M. Hossain, Radiation induced spent nuclear fuel dissolution under deep repository conditions, Environ. Sci. Technol. 41 (2007) 7087–7093.
[15] H. Christensen, S. Sunder, Current state of knowledge of water radiolysis effects on spent nuclear fuel corrosion, Nucl. Technol. 131 (2000) 102–103.
[16] B. Pastina, J. LaVerne, Effect of molecular hydrogen on hydrogen peroxide in water radyolisis, J. Phys. Chem. A 105 (2001) 9316–9322.
[17] S.D. Senanayake, R. Rousseau, D. Colegrave, H. Idriss, The reaction of water on polycrystalline UO_2: pathways to surface and bulk oxidation, J. Nucl. Mater. 342 (2005) 179–187.
[18] C. Ferry, C. Poinssot, C. Cappelaere, L. Desgranges, C. Jegou, F. Miserque, J. P. Piron, D. Roudil, J. Gras, Specific outcomes of the research on the spent fuel long-term evolution in interim dry storage and deep geological disposal, J. Nucl. Mater. 352 (2006) 246–253.
[19] L. Desgranges, H. Palancher, M. Gamaléri, J.S. Micha, V. Optasanu, L. Raceanu, T. Montesin, N. Creton, Influence of the U_3O_7 domain structure on cracking during the oxidation of UO_2, J. Nucl. Mater. 402 (2010) 167–172.
[20] H. Matzke, A. Turos, Mechanisms and kinetics of leaching of UO_2 in water, Solid State Ionics 49 (1991) 189–194.
[21] A. Turos, R. Falcone, A. Drigo, A. Sambo, L. Nowicki, N. Madi, J. Jagielski, H. J. Matzke, Structural transformations in leached uranium dioxide, Nucl. Instrum. Methods Phys. Res., Sect. B 118 (1996) 659–662.
[22] O. Roth, M. Jonsson, Oxidation of UO_2 (s) in aqueous solution, Cent. Eur. J. Chem. 6 (2008) 1–14.
[23] C. Frondel, Systematic mineralogy of uranium and thorium, U.S. Geol. Surv. Bull. 1064 (1958).
[24] C. Frondel, Mineral composition of gummite, Am. Mineral. 41 (1956) 539–568.
[25] I. Marchetti, Characterisation of Water Penetration into Polycrystalline UO_2, PhD Dissertation, Pisa, Italy, 2013.
[26] I. Marchetti, F. Belloni, J. Himbert, P. Carbol, T. Fanghanel, Novel insights in the study of water penetration into polycrystalline UO_2 by secondary ion mass spectrometry, J. Nucl. Mater. 408 (2011) 54–60.
[27] I. Marchetti, P. Carbol, J. Himbert, F. Belloni, T. Fanghänel, Room-temperature diffusion coefficients for oxygen and water in UO_2 matrices: a SIMS study, Surf. Interface Anal. 45 (2013) 360–363.
[28] I. Marchetti, F. Belloni, J. Himber, P. Carbol, T. Fanghänel, Characterization of the penetration mechanisms of water into polycrystalline UO_2, MRS Online Proceedings Library 1265 (2010) 706.
[29] E.C. Pearcy, J.D. Prikryl, W.M. Murphy, B.W. Leslie, Alteration of uraninite from the Nopal I deposit, Pena Blanca District, Chihuahua, Mexico, compared to degradation of spent nuclear fuel in the proposed U.S. high-level nuclear waste repository at Yucca Mountain, Nevada, app, Geochem. 9 (1994) 713–732.
[30] D. Zhao, R.C. Ewing, Alteration products of uraninite from the Colorado plateau, Radiochim. Acta 88 (2000) 739.
[31] A.P. Deditius, S. Utsunomiya, R.C. Ewing, Fate of trace elements during alteration of uraninite in a hydrothermal vein-type U-deposit from Marshall pass, Colorado, USA, Geochim. Cosmochim. Acta 71 (2007) 4954–4973.
[32] L. Perez del Villar, J. Bruno, R. Campos, P. Gomez, J.S. Cozar, A. Garralon, B. Buil, D. Arcos, G. Carretero, J. Ruiz Sanchez-Porro, P. Hernan, The uranium ore from Mina Fe (Salamanca, Spain) as a natural analogue of processes in a spent fuel repository, Chem. Geol. 190 (2002) 395–415.
[33] K.J. Cantrell, W.J. Deutsch, M.J. Lindberg, Thermodynamic model for uranium release from Hanford site tank residual waste, Environ. Sci. Technol. 45 (2011) 1473–1480.
[34] R. Fritsche, C. Sussieck-Fornefreld, Min-Petr. Inst., Univ Hedelberg, 2021. Germany.
[35] B.T.M. Willis, Structures of UO_2, UO_{2+x} and U_4O_9 by neutron diffraction, J. Phys. 25 (1964) 431–439.
[36] I. Cohen, R.M. Berman, A metallographic and X-ray study of the limits of oxygen solubility in the UO_2-ThO_2 system, J. Nucl. Mater. 18 (1966) 77–107.
[37] B.O. Loopstra, The phase transition in [alpha]-U_3O_8 at 210°C, J. Appl. Crystallogr. 3 (1970) 94–96.
[38] R.J. Finch, F.C. Hawthorne, R.C. Ewing, Structural relations among schoepite, metaschoepite and dehydrated schoepite, Can. Mineral. 36 (1998) 831–845.
[39] L.J. Bonales, C. Menor-Salván, J. Cobos, Study of the alteration products of a natural uraninite by Raman spectroscopy, J. Nucl. Mater. 462 (2015) 296–303.
[40] D. Manara, B. Renker, Raman spectra of stoichiometric and hyperstoichiometric uranium dioxide, J. Nucl. Mater. 321 (2003) 233–237.
[41] H. He, D. Shoesmith, Raman spectroscopic studies of defect structures and phase transition in hyper-stoichiometric UO_{2+x}, Phys. Chem. Chem. Phys. 12 (2010) 8108–8117.
[42] L. Desgranges, G. Baldinozzi, P. Simon, G. Guimbretiere, A. Canizares, Raman spectrum of U_4O_9: a new interpretation of damage lines in UO_2, J. Raman Spectrosc. 43 (2012) 455–458.
[43] I. Butler, G. Allen, N. Tuan, Micro-Raman Spectrum of Triuranium Octoxide, U_3O_8, Appl. Spectrosc. 42 (1988) 901–902.
[44] F. Pointurier, O. Marie, Identification of the chemical forms of uranium compounds in micrometer-size particles by means of micro-Raman spectrometry and scanning electron microscope, Spectrochim. Acta, B 65 (2010) 797–804.
[45] L. Maya, G.M. Begun, A Raman spectroscopy study of hydroxo and carbonato species of the uranyl (VI) ion, J. Inorg. Nucl. Chem. 43 (1981) 2827–2832.
[46] B.M. Biwer, W.L. Ebert, J.K. Bates, The Raman spectra of several uranylcontaining minerals using a microprobe, J. Nucl. Mater. 175 (1990) 188–193.
[47] M. Amme, B. Renker, B. Schmid, M.P. Feth, H. Bertagnolli, W. Döbelin, Raman microscpectrometric identification of corrosion products formed on UO_2 nuclear fuel during leaching experiments, J. Nucl. Mater. 306 (2000) 202–212.
[48] G. Lu, A.J. Haes, T.Z. Forbes, Detection and identification of solids, surfaces, and solutions of uranium using vibrational spectroscopy, Coord. Chem. Rev. 374 (2018) 314–344.
[49] E.A. Stefaniak, A. Alsecz, I.E. Sajo, A. Worobiec, Z. Mathe, S. Török, R.V. Grieken, Recognition of uranium oxides in soil particulate matter by means of μ-Raman spectrometry, J. Nucl. Mater. 381 (2008) 278–283.
[50] R.L. Frost, J. Cejka, M.L. Weier, Raman spectroscopic study of the uranyl oxyhydroxide hydrates: becquerelite, billietite, curite, schoepite and vandendriesscheite, J. Raman Spectrosc. 38 (2006) 460–466.
[51] M. Mellini, F. Riccobono, Chemical and mineralogical transformations caused by weathering in anti-tank DU penetrators ("the silver bullets") discharged during the Kosovo war, Chemosphere 60 (2005) 1246–1252.
[52] H.R. Hoekstra, S. Siegel, The uranium trioxide-water system, J. Inorg. Nucl. Chem. 35 (1973) 76l–779.
[53] J. Crank, The Mathematics of Diffusion, second ed., Oxford University Press, Oxford, 1975.
[54] K.W. Lay, Oxygen chemical diffusion coefficient of uranium dioxide, J. Am. Ceram. Soc. 53 (1970) 369–373.
[55] A. Poulesquen, L. Desgranges, C. Ferry, An improved model to evaluate the oxidation kinetics of uranium dioxide during dry storage, J. Nucl. Mater. 362 (2007) 402–410.
[56] M. Fayek, T.K. Kyser, Low temperature oxygen isotopic fractionation in the uraninite-UO_2-CO_2-H_2O system, Geochim. Cosmochim. Acta 64 (2000) 2185–2197.
[57] L.J. Bonales, C. Menor-Salván, J. Cobos, Study of the alteration products of a natural uraninite by Raman spectroscpy, J. Nucl. Mater. 432 (2015) 296–303.
[58] N.J. Mendoza, L.J. Bonales, V.G. Baonza, M. Cáceres, Local hydration pressures in methanol aqueous solution: a Raman spectroscopy analysis, J. Phys. Chem. B 118 (2014) 9919–9925.